ANALYSIS OF PYROCLASTIC DEPOSITS WITHIN GAUSS CRATER. J.Olaf Gustafson[1], L.R. Gaddis[2], and T.A. Giguere[3]. [1]Dept. Earth & Atmospheric Sciences, Cornell University, Ithaca, NY; [2]Astrogeology Science Center, U.S. Geological Survey, Flagstaff, AZ; [3]Hawaii Institute of Geophysics and Planetology, University of Hawaii, Honolulu, HI. (jg72@cornell.edu).

Introduction: Numerous localized pyroclastic deposits have been identified within the Nectarian floor-fractured crater Gauss (D= 177 km), located in the highlands northeast of Mare Crisium (36.0°N, 79.0°E)[1,2]. Recent data from the camera subsystems aboard the Lunar Reconnaissance Orbiter (LRO) and SELENE/Kaguya spacecraft [3-5] enable more detailed analysis of these pyroclastic deposits. We use regional mosaics from the LRO Wide Angle Camera (WAC) to analyze the geologic setting; high-resolution monochrome data from the LRO Narrow Angle Camera (NAC; resolution ~0.5-2.0 m/pixel) to examine deposit morphologies, surface textures, and potential source vents; and multispectral data from the Kaguya Multiband Imager (MI; five visible and near-infrared wavelengths from 415-1000 nm; resolution ~20 m/px) to constrain deposit compositions and look for differences in mineralogy and/or glass content between deposits. We also use derived products from these data, including the WAC GLD100 digital terrain model (DTM) [6] and mineral maps derived from Kaguya MI data [7,17].

Background: Lunar pyroclastic deposits (LPDs) have been identified across the Moon, often based on their low albedo, smooth texture, and mantling effect over underlying terrain features [8-10]. The composition and distribution of these materials provide important clues to the history of lunar volcanism and the composition of the interior. Analysis of pyroclastic glass samples has indicated that many are enriched in metallic and volatile elements (e.g. Fe, Ti, Zn, S), and they are of interest both as samples of the lunar interior and as potential targets for resource extraction [11-13]. Deposits of both regional (roughly >1000 km^2) and localized (tens to hundreds of km^2) extent have been documented; localized deposits are often associated with endogenic craters or depressions [9,14].

Gauss (Fig. 1) is one of several highland craters north of Crisium that contains pyroclastic deposits; others include Messala, Franklin, and floor-fractured Atlas [14]. Three groups of pyroclastic vents and associated deposits have been identified (Fig. 2): a western cluster of two deposits along a prominent rille; a southern cluster of 3 deposits within and near Gauss G; and an eastern cluster of two deposits along rilles within Gauss B [2,14].

Results and Discussion: In a similar manner to other floor-fractured craters, Gauss exhibits a slightly domed floor with circumferential moats (Fig.1). This morphology has been interpreted to be the result of magmatic intrusion beneath the crater floor [15,16]. The pyroclastic deposits are located along rilles and in topographic lows, locations where magmatic overpressure could most easily drive eruptions at the surface.

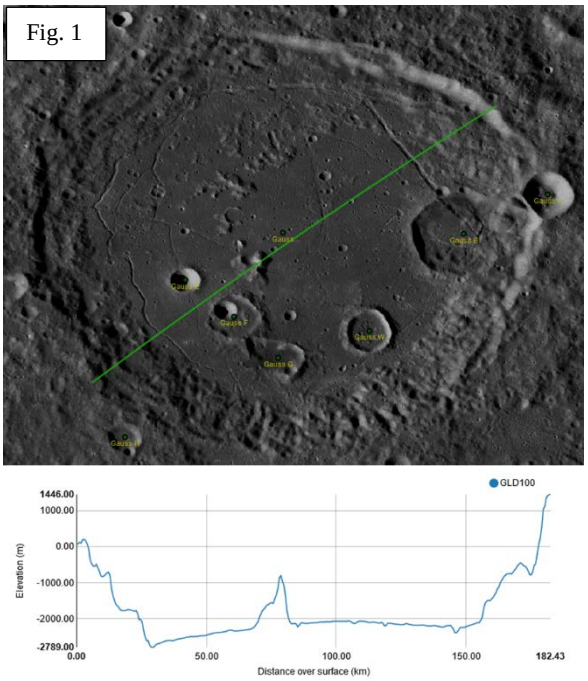

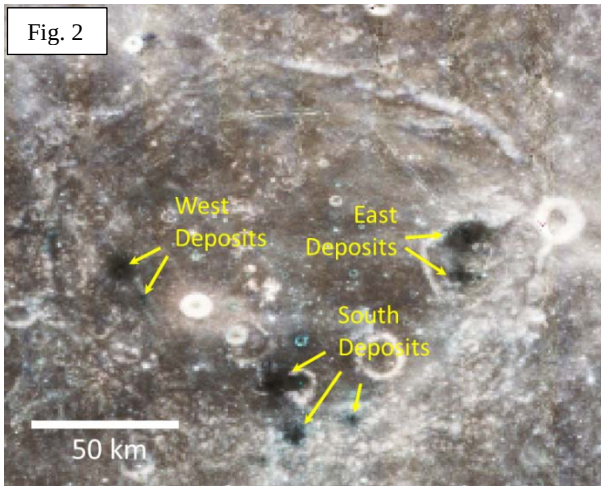

Fig. 1 – Portion of WAC global mosaic and GLD100 topographic profile (green line). (NASA/GSFC/ASU)
Fig. 2 - Kaguya MI color image of the Gauss pyroclastic deposits (arrows). R=1000 nm, G=750 nm, B=415 nm. (JAXA)

Mineral abundance maps produced from the Kaguya MI data [17] show that the pyroclastic deposits contain a significant component of olivine (~11-23%) along

with orthopyroxene (~4-16%) and clinopyroxene (~0.5-9%), in addition to plagioclase (~60-76%). However, recent studies have suggested that what has been interpreted as olivine in lunar pyroclastic deposits is more likely a glass component [18-20]. For this analysis we have chosen to interpret the MI-derived olivine concentrations as pyroclastic glass, although the actual abundance of such material is uncertain. The glass component of the pyroclastic deposits produces a strong spectral signature (Fig. 3).

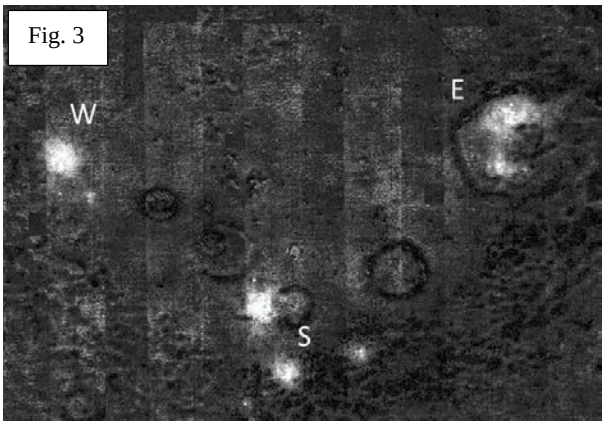

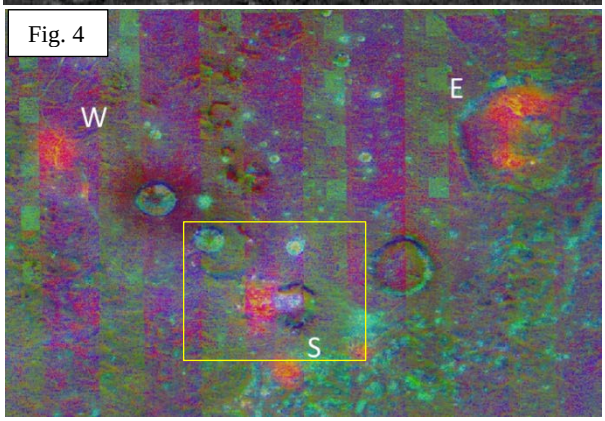

Fig. 3 – Kaguya MI derived olivine [17], used here as a proxy for relative glass abundance.
Fig. 4 – Color composite image where MI-derived glass proxy = red, OPX = green, and CPX = blue. Yellow box shows location of Fig. 5. (JAXA)

The image in Figure 4 was created by combining the MI-derived glass proxy (red), orthopyroxene (OPX, green), and clinopyroxene (CPX, blue) abundances, which reveals compositional differences between crater floor units (OPX), LPDs (juvenile glass, CPX) and gradients within them. One notable observation from this composite image is that the main southern deposit has very different western and eastern portions. The western portion is dominated by a glass component, while the eastern portion is dominated by clinopyroxene. Inspection of the WAC mosaic (Fig. 5) indicates that the eastern portion of the deposit is a smooth, effusive unit, while the western portion is dominated by pyroclastic material. This southern deposit represents an unusual association of effusive (lava flow and mare pond) and explosive volcanism that is rare among the LPDs [14]. Eruption and emplacement of these deposits likely is more complex and diverse than previously thought.

Summary and Future Work: The use of the LROC WAC, NAC, and Kaguya MI data sets for analysis of localized pyroclastic deposits is facilitating more detailed characterization of the extent, morphology, and composition of these materials. Future work will include more detailed analysis of variations within individual deposits, as well as between multiple related pyroclastic deposits and between pyroclastics and nearby effusive deposits, in order to further our understanding of magma sources and eruption mechanisms. Further refinement of analysis techniques for the available lunar multispectral data sets will enable more nuanced interpretations of the mineralogy and geologic history of these important volcanic features.

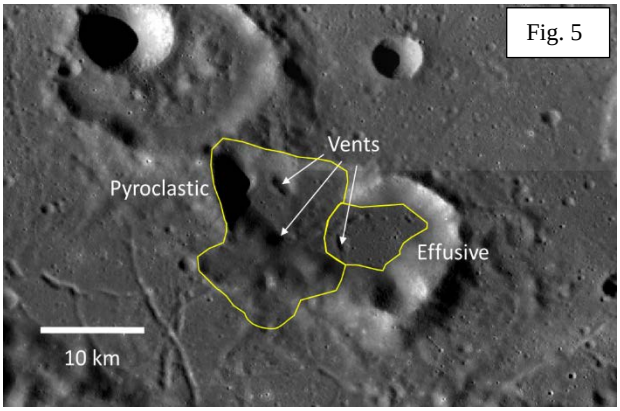

Fig. 5 – Portion of WAC mosaic showing main South deposit; the pyroclastic western portion can be differentiated from the smooth effusive eastern portion. (NASA/GSFC/ASU)

References: [1] Hawke & Head (1980) *LPS 6th*, 416-417; [2] Hawke *et al.* (2013) *LPS 44th* #1883; [3] Robinson *et al.* (2010) *Space Sci. Rev. 150* (1-4), 81-124; [4] Haruyama *et al.* (2008) *Adv. Sp. Res. 42*, 310-316; [5] Ohtake *et al.* (2010) *Space Sci. Rev. 154*, 57-77; [6] Scholten *et al.* (2012) *JGR 117*, E00H17; [7] Otake *et al.* (2012) *LPS 43rd* #1905; [8] Head (1974) *PLSC 5th*, 207-222; [9] Gaddis *et al.* (1985) *Icarus 61*, 461-488; [10] Hawke *et al.* (1989) *LPS 19th*, 255-268; [11] Heiken *et al.* (1974) *GCA 38*, 1703; [12] Delano (1986) *JGR 91*, D201; [13] Hawke *et al.* (1990) *LPS 20th*, 249; [14] Gaddis *et al.* (2003) *Icarus 161*, 262-280; [15] Schultz (1976) *Moon 15*, 241-273; [16] Joswiak *et al.* (2012) *JGR 117*, E11005; [17] Lemelin *et al.* (2016) *LPS 47th* #2994; [18] Horgan *et al.* (2014) *Icarus 234*, 132-154; [19] Jawin *et al.* (2015) *JGR 120*, 1310-1331; [20] Trang *et al.* (2017) *Icarus 283*, 232-253.